Correlation Functions, Universal Ratios and Goldstone Mode Singularities in n-Vector Models

J. Kaupužs[1,2,*], R. V. N. Melnik[3] and J. Rimšāns[1,2]

[1] *Institute of Mathematics and Computer Science, University of Latvia, 29 Raiņa Boulevard, LV1459, Riga, Latvia.*
[2] *Institute of Mathematical Sciences and Information Technologies, University of Liepaja, 14 Liela Street, Liepaja LV-3401, Latvia.*
[3] *Wilfrid Laurier University, Waterloo, Ontario, Canada, N2L 3C5.*

Abstract. Correlation functions in the $\mathcal{O}(n)$ models below the critical temperature are considered. Based on Monte Carlo (MC) data, we confirm the fact stated earlier by Engels and Vogt, that the transverse two-plane correlation function of the $\mathcal{O}(4)$ model for lattice sizes about $L=120$ and small external fields h is very well described by a Gaussian approximation. However, we show that fits of not lower quality are provided by certain non-Gaussian approximation. We have also tested larger lattice sizes, up to $L=512$. The Fourier-transformed transverse and longitudinal two-point correlation functions have Goldstone mode singularities in the thermodynamic limit at $k \to 0$ and $h = +0$, i.e., $G_\perp(\mathbf{k}) \simeq ak^{-\lambda_\perp}$ and $G_\parallel(\mathbf{k}) \simeq bk^{-\lambda_\parallel}$, respectively. Here a and b are the amplitudes, $k=|\mathbf{k}|$ is the magnitude of the wave vector $\mathbf{k}$. The exponents $\lambda_\perp$, $\lambda_\parallel$ and the ratio bM^2/a^2, where M is the spontaneous magnetization, are universal according to the GFD (grouping of Feynman diagrams) approach. Here we find that the universality follows also from the standard (Gaussian) theory, yielding $bM^2/a^2=(n-1)/16$. Our MC estimates of this ratio are 0.06 ± 0.01 for $n=2$, 0.17 ± 0.01 for $n=4$ and 0.498 ± 0.010 for $n=10$. According to these and our earlier MC results, the asymptotic behavior and Goldstone mode singularities are not exactly described by the standard theory. This is expected from the GFD theory. We have found appropriate analytic approximations for $G_\perp(\mathbf{k})$ and $G_\parallel(\mathbf{k})$, well fitting the simulation data for small k. We have used them to test the Patashinski-Pokrovski relation and have found that it holds approximately.

*Corresponding author. *Email addresses:* `kaupuzs@latnet.lv` (J. Kaupužs), `rmelnik@wlu.ca` (R. Melnik), `rimshans@mii.lu.lv` (J. Rimšāns)

1   Introduction

The n-component vector-spin models (called also n-vector models or $\mathcal{O}(n)$ models), have attracted significant interest in recent decades as the models, where the so-called Goldstone mode singularities are observed. The Hamiltonian of the n-vector model $\mathcal{H}$ is given by

$$\frac{\mathcal{H}}{T} = -\beta\Big(\sum_{\langle ij\rangle}\mathbf{s}_i\mathbf{s}_j + \sum_i\mathbf{h}\mathbf{s}_i\Big), \tag{1.1}$$

where T is temperature, $\mathbf{s}_i \equiv \mathbf{s}(\mathbf{x}_i)$ is the n-component vector of unit length, i.e., the spin variable of the i-th lattice site with coordinate $\mathbf{x}_i$, β is the coupling constant, and $\mathbf{h}$ is the external field. The summation takes place over all nearest neighbors in the lattice. Periodic boundary conditions are considered here.

In the thermodynamic limit below the critical temperature (at $\beta > \beta_c$), the magnetization $M(h)$ (where $h = |\mathbf{h}|$), the Fourier-transformed transverse ($G_\perp(\mathbf{k})$) and longitudinal ($G_\parallel(\mathbf{k})$) two-point correlation functions exhibit Goldstone mode power-law singularities:

$$M(h) - M(+0) \propto h^\rho \qquad \text{at } h \to 0, \tag{1.2a}$$

$$G_\perp(\mathbf{k}) = ak^{-\lambda_\perp} \qquad \text{at } h = +0 \quad \text{and} \quad k \to 0, \tag{1.2b}$$

$$G_\parallel(\mathbf{k}) = bk^{-\lambda_\parallel} \qquad \text{at } h = +0 \quad \text{and} \quad k \to 0, \tag{1.2c}$$

with certain exponents ρ, $\lambda_\perp$, $\lambda_\parallel$ and the amplitudes a, b of the Fourier-transformed two-point correlation functions.

In a series of theoretical works (e.g., [1–11]), it has been claimed that the exponents in (1.2a)-(1.2c) are exactly $\rho = 1/2$ at $d = 3$, $\lambda_\perp = 2$ and $\lambda_\parallel = 4 - d$, where d is the spatial dimensionality $2 < d < 4$. These theoretical approaches are further referred here as the standard theory. Several MC simulations have been performed earlier [12–15] to verify the compatibility of MC data with standard-theoretical expressions, where the exponents are fixed. In recent years, we have performed a series of accurate MC simulations [16–19] for remarkably larger lattices than previously were available, with an aim to evaluate the exponents in (1.2a)-(1.2c). Some deviations from the standard-theoretical values have been observed, in agreement with an alternative theoretical approach, known as the GFD (grouping of Feynman diagrams) theory [20], where the relations $d/2 < \lambda_\perp < 2$, $\lambda_\parallel = 2\lambda_\perp - d$ and $\rho = (d/\lambda_\perp) - 1$ have been found for $2 < d < 4$.

In the GFD theory, the perturbation theory is reorganized in such a way that all Feynman diagrams are summed up into certain skeleton diagrams, where the true correlation function (instead of the Gaussian one) corresponds to the coupling lines. Further grouping and resummation of all these skeleton diagrams allows us to perform a qualitative analysis without cutting the perturbation series. Possible reasons for discrepancies between the GFD theory and standard perturbative treatments are discussed in [18]. This discussion is mainly devoted to the critical point singularities, but the same arguments refer also to the Goldstone mode singularities. There are some difficulties in the GFD

analysis [18], since it is not possible to sum up all skeleton diagrams and write down precisely the complete result (only certain scaling forms can be derived). On the other hand, a real failure of a standard perturbative treatment (ε-expansion) has been recently detected in [21]. The reason of such a failure, likely, is the formal character of the expansions commonly used in the standard perturbative approaches [18, 21].

Here we focus on the relations, which have not been tested in the previous MC studies (see Section 2). In particular, the two-plane correlation function, studied in [15], is re-examined in Section 3. Furthermore, we have also evaluated in Section 4 the universal ratio bM^2/a^2 for $n=2,4,10$ and have compared the MC estimates with the values calculated here from the standard theory. Finally, in Section 5 we have proposed and tested certain analytical approximations for the two-point correlation functions, and in Section 6 have tested the Patashinski-Pokrovski relation (PP relation).

2   Correlation functions

In presence of an external field **h**, the longitudinal (parallel to **h**) and the transverse (perpendicular to **h**) spin components have to be distinguished. The Fourier-transformed longitudinal and transverse two-point correlation functions are

$$G_j(\mathbf{k}) = \sum_{\mathbf{x}} \grave{G}_j(\mathbf{x}) e^{-i\mathbf{k}\mathbf{x}}, \tag{2.1}$$

where $j=1$ refers to the longitudinal component and $j=2,\cdots,n$ — to the transverse ones. Here

$$\grave{G}_j(\mathbf{x}) = \langle s_j(\mathbf{0}) s_j(\mathbf{x}) \rangle \tag{2.2}$$

are the two-point correlation functions in the coordinate space. (Note that the factor N^{-1} in Eqs. (1.2)-(1.3) of [19] and (28)-(29) of [18] is $N^{-1}=1$ according to the actual definitions (2.1)-(2.2).) The inverse transform of (2.1) is

$$\grave{G}_j(\mathbf{x}) = L^{-3} \sum_{\mathbf{k}} G_j(\mathbf{k}) e^{i\mathbf{k}\mathbf{x}}, \tag{2.3}$$

where L is the linear lattice size. In the following, the cumulant correlation function

$$\tilde{G}_j(\mathbf{x}) = \langle s_j(\mathbf{0}) s_j(\mathbf{x}) \rangle - \langle s_j(\mathbf{0}) \rangle \langle s_j(\mathbf{x}) \rangle \tag{2.4}$$

will also be considered. It agrees with $\grave{G}_j(\mathbf{x})$ for the transverse components, whereas a nonzero constant contribution $\langle s_1 \rangle^2 = M^2$ is subtracted in the longitudinal case.

Following [15], the two-plane correlation function is defined as

$$D_j(\tau) = L^2 \langle S_j(0) S_j(\tau) \rangle, \tag{2.5}$$

where

$$S_j(\tau) = L^{-2} \sum_{x,y=0}^{L-1} s_j(x,y,\tau) \tag{2.6}$$

is the spin component s_j, which is averaged over the plane $z = \tau$, denoting $\mathbf{x} = (x, y, \tau)$.

Using the definition of $D_j(\tau)$, as well as the relations (2.2) and (2.3), we obtain

$$
\begin{aligned}
D_j(\tau) &= \sum_{x,y=0}^{L-1} \grave{G}_j(x,y,\tau) \\
&= L^{-3} \sum_{m_1,m_2,m_3} \sum_{x,y=0}^{L-1} G_j(k_{m_1}, k_{m_2}, k_{m_3}) \exp\left[\frac{2\pi i}{L}(m_1 x + m_2 y + m_3 \tau)\right],
\end{aligned} \tag{2.7}
$$

where $\grave{G}_j(x,y,\tau) \equiv \grave{G}_j(\mathbf{x})$ with $\mathbf{x} = (x,y,\tau)$ and $G_j(k_{m_1}, k_{m_2}, k_{m_3}) \equiv G_j(\mathbf{k})$ with $\mathbf{k} = (k_{m_1}, k_{m_2}, k_{m_3})$, $k_m = 2\pi m/L$. The summation over indices m_j goes from $1 - L + [L/2]$ to $[L/2]$, where $[L/2]$ denotes the integer part of $L/2$. According to the properties of the wave function $\exp[2\pi i L^{-1}(m_1 x + m_2 y + m_3 \tau)]$, the summation over x and y gives vanishing result unless $m_1 = m_2 = 0$. More precisely, it leads to the result

$$
D_j(\tau) = \frac{1}{L} \sum_\ell G_j(k_\ell) \cos(k_\ell \tau), \tag{2.8}
$$

where $G_j(k) \equiv G_j(0,0,k)$ is the Fourier-transformed two-point correlation function in the $\langle 100 \rangle$ crystallographic direction, and $k_\ell = 2\pi \ell / L$ with $\ell \in [1 - L + [L/2], [L/2]]$.

The Gaussian approximation for $D_j(\tau)$ can be obtained from the Gaussian model, where fluctuations of each of the transverse components $\varphi_j(\mathbf{x})$ of the order-parameter field $\varphi(\mathbf{x})$ are described by a part of Hamiltonian $2^{-1} \sum_{\mathbf{x}} \left(a \varphi_j^2(\mathbf{x}) + c(\nabla \varphi_j(\mathbf{x}))^2\right)$. Here the sum runs over discrete lattice with the lattice constant of unit length, whereas $\varphi_j(\mathbf{x})$ is considered as a smooth function according to the Fourier representation $\varphi_j(\mathbf{x}) = N^{-1/2} \sum_{\mathbf{k}} \varphi_{\mathbf{k},j} e^{i\mathbf{k}\mathbf{x}}$, where N is the total number of lattice sites. This part of Hamiltonian reduces to $2^{-1} \sum_{\mathbf{k}} (a + ck^2) |\varphi_{\mathbf{k},j}|^2$ (since $\varphi_j(\mathbf{x})$ is real and therefore $\varphi_{-\mathbf{k},j} = \varphi_{\mathbf{k},j}^*$ holds), provided that the wave vectors $\mathbf{k}/(2\pi)$ belong to a unit cube centered at $\mathbf{k} = \mathbf{0}$. Hence, the transverse Gaussian two-point correlation function is

$$
G_\perp^{\text{Gauss}}(\mathbf{k}) = \frac{1}{a + ck^2} = \frac{\chi_\perp m^2}{m^2 + k^2}. \tag{2.9}
$$

The parameter $m = \sqrt{a/c}$ (for $a \geq 0$) in (2.10) is interpreted as mass, and the known relation $G_\perp(0) = \chi_\perp$ between the transverse correlation function $G_\perp(0)$ and the transverse susceptibility $\chi_\perp$ is used here. The corresponding transverse two-plane correlation function in the Gaussian approximation

$$
D_\perp^{\text{Gauss}}(\tau) = \frac{\chi_\perp}{L} \sum_\ell \frac{m^2}{m^2 + k_\ell^2} \cos(k_\ell \tau) \tag{2.10}
$$

is obtained by setting (2.10) into (2.8).

According to the given here consideration, the approximation (2.9) is meaningful for a discrete lattice only if the wave-vector components belong to the interval $[-\pi,\pi]$. Therefore, the summation limits in (2.10) are chosen such that $k_\ell \leq \pi$, and they cannot be arbitrarily shifted.

The true correlation function (2.1) is invariant with respect to the shift of any component of the wave vector $\mathbf{k}$ by 2π. Besides, $G_\perp(k) \equiv G_\perp(0,0,k)$ is symmetric with respect to $k = \pi$ and is smooth around $k = \pi$ — see, e.g., Fig. 5 in [17]. A modified Gaussian approximation

$$\tilde{G}_\perp^{\mathrm{Gauss}}(\mathbf{k}) = \frac{\chi_\perp m^2}{m^2 + \tilde{k}^2} \tag{2.11}$$

with

$$\tilde{k}^2 = (2\sin(k_x/2))^2 + (2\sin(k_y/2))^2 + (2\sin(k_z/2))^2, \tag{2.12}$$

(here $\mathbf{k} = (k_x,k_y,k_z)$) has these properties and reduces to (2.9) at small k. The corresponding modified Gaussian approximation for $D_\perp(\tau)$ is

$$\tilde{D}_\perp^{\mathrm{Gauss}}(\tau) = \frac{\chi_\perp}{L} \sum_\ell \frac{m^2}{m^2 + \tilde{k}_\ell^2} \cos(k_\ell \tau) \tag{2.13}$$

with $\tilde{k}_\ell^2 = (2\sin(k_\ell/2))^2$. In distinction from (2.10), the summation limits for ℓ in (2.8) and (2.13) can be shifted by any integer number.

A different from (2.10) formula has been also proposed in [15], i.e.,

$$D_\perp^{\mathrm{Eng}}(\tau) = \chi_\perp \tanh\left(\frac{m}{2}\right) \frac{e^{-m\tau} + e^{-m(L-\tau)}}{1 - e^{-mL}}. \tag{2.14}$$

Eq. (2.14) is obtained assuming that $D_\perp(\tau)$ is proportional to $e^{-m\tau} + e^{-m(L-\tau)}$ [15], as in the case of the continuum limit, where the summation over wave vectors $2\pi\ell/L$ runs from $\ell = -\infty$ to $\ell = \infty$. Besides, the proportionality coefficient is determined from the normalization condition

$$\sum_{\tau=0}^{L-1} D_\perp(\tau) = \chi_\perp. \tag{2.15}$$

Note that this condition is automatically satisfied in (2.8), (2.10) and (2.13) according to $G_\perp(0) = \chi_\perp$, since all terms cancel each other after the summation over τ, except only those with $k = 0$. It is clear that (2.14) is not exactly consistent with (2.10), as it can be easily checked by writing down all terms in (2.10), e.g., at $L = 2$ (where only terms with $\ell = 0$ and $\ell = 1$ appear). However, the difference appears to be rather small for large L and small m. In Fig. 1, we have shown the ratio $D_\perp^{\mathrm{Eng}}(\tau)/D_\perp^{\mathrm{Gauss}}(\tau)$ for the lattice size $L = 120$ simulated in [15] at a typical value of mass $m = 0.02$ considered there. As we can see, the largest difference, about 0.3%, appears at $\tau = 0$. In fact, the approximation (2.14) is very similar to (2.13). Indeed, the ratio $D_\perp^{\mathrm{Eng}}(\tau)/\tilde{D}_\perp^{\mathrm{Gauss}}(\tau)$ changes monotonously from $1.0000093475\cdots$ at $\tau = 0$ to $0.9999926752\cdots$ at $\tau = 60$.
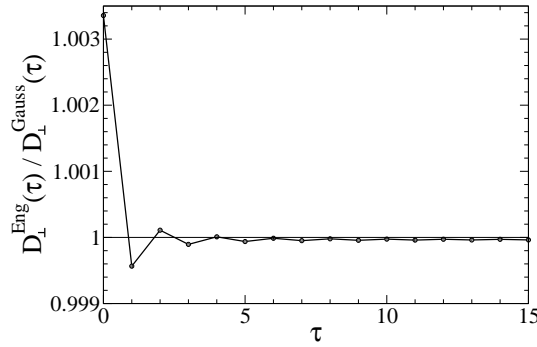
Figure 1: The ratio $D_\perp^{\text{Eng}}(\tau)/D_\perp^{\text{Gauss}}(\tau)$ calculated from (2.14) and (2.10) for $m=0.02$ and $L=120$ within $0 \le \tau \le 15$.

It turns out that (2.13) and (2.14) slightly better than (2.10) fit the simulation data around $\tau=0$, although the quality of the overall fit is practically the same.

It is interesting to mention that $D_\perp^{\text{Eng}}(\tau)$ corresponds to certain approximation for $G_j(k) = G_\perp(k)$ in (2.8), i.e., to

$$G_\perp^*(k) = \frac{2}{m}\tanh\left(\frac{m}{2}\right) \sum_{j'=-\infty}^{\infty} G_\perp^{\text{Gauss}}(k+2\pi j'). \qquad (2.16)$$

Indeed, an infinite sum over all integer values of ℓ is obtained when inserting the approximation (2.16) for $G_\perp(k)$ into (2.8), yielding (2.14) (see [15] for treatment of such sums). The correct normalization is ensured here by the factor $2m^{-1}\tanh(m/2)$ in (2.16). Like (2.11), the approximation (2.16) has the correct periodicity, as well as the symmetry and smoothness property around $k=\pi$. An obvious advantage of the approximation (2.11) as compared to (2.16) is that (2.11) is valid for an arbitrary wave vector $\mathbf{k}$, whereas (2.16)-only for a vector oriented along one of the axes.

Within the interval $k \in [0,\pi]$, the approximations (2.11) and (2.16) remarkably differ from (2.9) only at large wave vectors $k \sim \pi$. Therefore, the most significant difference between (2.13) and (2.10) or (2.14) and (2.10) appears at small τ values.

3 Fits of the two-plane correlation function

The two-point correlation functions $G_j(k)$ for $n=2,4,10$ have been extracted from MC simulations by a modified Wolff cluster algorithm in our earlier works [17–19]. According to (2.8), it allows us to evaluate also the two-plane correlation functions and compare the results and conclusions with those of [15]. In this case, it is meaningful to determine the $G_\perp(0)$ value from the relation

$$G_\perp(0) = \chi_\perp = \frac{M(h)}{\beta h}, \qquad (3.1)$$

which holds owing to the rotational symmetry of the model. The statistical error for $\chi_\perp$, calculated as $M(h)/(\beta h)$, is much smaller than that for $\chi_\perp^* = G_\perp(0)$, calculated from the common formulas for $G_\perp(k)$ in [17], although the agreement within the error bars is expected according to (3.1).

Our simulations have been performed in the ordered phase not close to the critical point $\beta = \beta_c$. According to the estimates given in [23], the critical couplings β_c of the $\mathcal{O}(n)$ models are 0.2216544(3) for $n=1$, 0.45419(3) for $n=2$, 0.69305(4) for $n=3$ and 0.93600(4) for $n=4$. Besides, $\beta_c(n) > const \cdot n \ln n$ holds [24], which means that the critical temperature $T_c = 1/\beta_c$ vanishes at $n \to \infty$. The listed here estimates of [23] show an almost proportional to $1/n$ behavior of T_c. Hence the linear interpolation between $1/n = 0.25$ and $1/n = 0$ (where $T_c = 0$) gives a rough estimate $\beta_c \approx 2.34$ for $n = 10$. The latter value of β_c might be slightly larger because of a small curvature of the T_c vs $1/n$ plot. Our simulations have been performed at $\beta = 0.55$ for $n=2$; $\beta = 1.1$ and $\beta = 1.2$ for $n=4$; and $\beta = 3$ for $n = 10$. The corresponding reduced temperatures $\beta/\beta_c - 1$ range from 0.175 to 0.282. Besides, the values of spontaneous magnetization are not small, i.e., around 0.5, giving a clear evidence that the simulations have been performed not close to the critical point. It allows us to avoid possible crossover effects [1, 4, 22], related to an interpolation between the Goldstone-mode behavior and the critical-point behavior. For comparison, a small reduced temperature about 0.00437, corresponding to $\beta = 0.94$ in the $\mathcal{O}(4)$ model, has been considered in [15] to see the influence of the critical fluctuations. Our simulations have been performed also at not large values of β/β_c to avoid possible low-temperature effects. Indeed, the Gaussian spin-wave theory is known to be asymptotically exact at low temperatures $T \to 0$. According to [20], it means that some crossover from the Gaussian to a non-Gaussian behavior is expected at a low temperature and small wave vectors, since the asymptotic behavior at $k \to 0$ (at $L = \infty$ and $h = +0$) is predicted to be non-Gaussian for a finite T.

We have calculated $D_\perp(\tau)$ (equal to $D_j(\tau)$ for $j \geq 2$) from (2.8) and have fit the results to the modified Gaussian form (2.13) (the fits to (2.10) give practically the same results) with $\chi_\perp$ being determined directly from simulations as $M(h)/(\beta h)$. In this case, the only fit parameter is m. Our fit results for m, together with the above discussed values of $\chi_\perp$ and $\chi_\perp^*$ for $\mathcal{O}(n)$ models with $n = 2,4,10$ are collected in Tables 1 to 3. The results for different lattice sizes L at the smallest h values in our simulations are shown here, providing also the χ^2/d.o.f. (χ^2 of the fit per degree of freedom) values, characterizing the quality of the fits. A comparison between $\chi_\perp$ and $\chi_\perp^*$ for the $\mathcal{O}(4)$ model has been provided already in [17]. In distinction from [17], here we do not use extra runs for $\chi_\perp$, i.e., both quantities are extracted from the same simulation runs.

We have found it convenient to split any simulation run in 110 bins, each including about $7.7 \times 10^5/L$ cluster algorithm steps, discarding first 10 bins for equilibration [17]. The statistical error of a quantity X is evaluated by the jackknife method [25] as $\sqrt{\sum_i (X - X_i)^2}$, where X_i is the X value, obtained by omitting the i-th bin. Here the bin-averages are considered as statistically independent (or almost independent) quantities. It is well justified, since the number of MC steps of one bin is much larger than that of the

Table 1: The estimates of transverse susceptibility $\chi_\perp$ and $\chi_\perp^*$ (see text) and the fit parameter m (mass) in (2.13) for the $\mathcal{O}(2)$ model at $\beta = 0.55$ and $h = 0.00021875$ depending on the lattice size L. The values of $\chi^2/$d.o.f. of the fit are given in the last column.

L	m	$\chi_\perp$	$\chi_\perp^*$	$\chi^2/$d.o.f.
512	0.01714(41)	5254.762(75)	4645(387)	1.24
384	0.01681(44)	5254.765(79)	5236(368)	0.67
256	0.01690(25)	5254.22(19)	5846(445)	1.27
128	0.01717(16)	5245.68(67)	5321(212)	0.91
64	0.016723(76)	5142.7(1.5)	5230(60)	0.11

Table 2: The susceptibility estimates $\chi_\perp$ and $\chi_\perp^*$, the fit parameter m in (2.13), and the $\chi^2/$d.o.f. values of the fit for the $\mathcal{O}(4)$ model at $\beta = 1.1$ and $h = 0.0003125$ vs size L.

L	m	$\chi_\perp$	$\chi_\perp^*$	$\chi^2/$d.o.f.
350	0.02380(41)	1422.831(40)	1449(75)	1.01
256	0.02423(34)	1422.775(60)	1435(64)	0.28
128	0.02398(16)	1420.98(18)	1404(42)	0.36
64	0.024019(92)	1389.21(57)	1386(16)	0.074

Table 3: The susceptibility estimates $\chi_\perp$ and $\chi_\perp^*$, the fit parameter m in (2.13), and the $\chi^2/$d.o.f. values of the fit for the $\mathcal{O}(10)$ model at $\beta = 3$ and $h = 0.00021875$ vs size L.

L	m	$\chi_\perp$	$\chi_\perp^*$	$\chi^2/$d.o.f.
350	0.02042(28)	719.464(24)	732(28)	4.61
256	0.02147(27)	719.468(36)	665(25)	1.28
192	0.02086(19)	719.176(58)	744(24)	0.27
128	0.02102(12)	717.47(14)	715(19)	0.18
64	0.021505(71)	690.07(36)	694.8(6.2)	0.097

autocorrelation time. We have verified it by checking that the estimated statistical errors are practically the same when twice larger bins are used. The discarded 10 bins comprise a remarkable fraction of a simulation. It ensures a very accurate equilibration. We have verified it by comparing the estimates extracted from separate parts of a simulation. The statistical errors in $G_\perp(k)$ at different k values are correlated, since $G_\perp(k)$ is measured simultaneously for all k. Hence, the statistical errors in $D_\perp(\tau)$ are correlated, as well.

The obtained values of m are almost independent of L for $L \geq 128$ (or even for $L \geq 64$ in Table 2). It means that the thermodynamic limit is practically reached here. It is understandable, since the lattice size L in these cases is remarkably larger than the transverse correlation length, which is approximately $1/m$ (in fact, the approximation $G_\perp(k) \propto 1/(m^2 + k^2)$ for small k gives the second momentum correlation length $1/m$, but the exponential correlation length is similar — see, e.g., [15]).
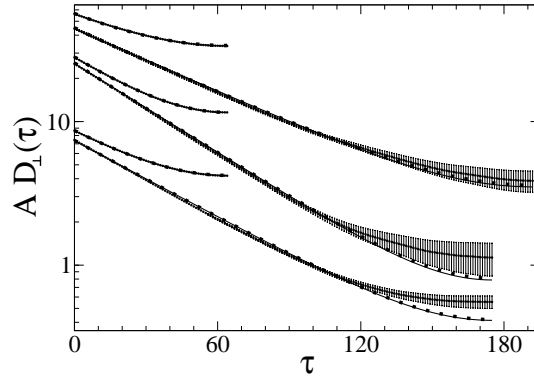
Figure 2: $AD_\perp(\tau)$ vs τ plots of the transverse two-plane correlation function $D_\perp(\tau)$ in the $\mathcal{O}(n)$ model. The results are shown for $n=2$ (upper plots, $A=1$, $\beta=0.55$, $h=0.00021875$, $L=128$ and 384), $n=4$ (middle plots, $A=1.5$, $\beta=1.1$, $h=0.0003125$, $L=128$ and 350), and $n=10$ (lower plots, $A=1$, $\beta=3$, $h=0.00021875$, $L=128$ and 350). The curves extend to $\tau \le L/2$. The solid lines are fits to the modified Gaussian form (2.13), the dotted lines — fits to (2.8) with the approximation (3.2) for $G_\perp(k)$, where $\lambda_\perp=1.929, 1.955, 1.972$ for $n=2,4,10$, respectively.

The $D_\perp(\tau)$ fits to the ansatz (2.13) for $L=128$ and for a larger size, $L=350$ or $L=384$, are plotted by solid lines in Fig. 2. The fits look perfect for $L=128$ (short curves). In such a way, we confirm the results of [15], where perfect fits for a similar size $L=120$ have been obtained in the case of $n=4$. However, our fits are less perfect for larger sizes (longer curves). In the cases of $n=2$ and $n=4$, the discrepancies about one standard error can be explained by correlated statistical errors in the $D_\perp(\tau)$ data. However, the deviations of the data points from the fit curve are remarkably larger for $n=10$ and $L=350$, as it can be seen from the lower plots in Fig. 2, as well as from the relatively large $\chi^2/$d.o.f. value 4.61 in this case — see Table 3.

The authors of [15] tend to interpret the very good fits of $D_\perp(\tau)$ to the ansatz (2.14) for the $\mathcal{O}(4)$ model at $L=120$ as an evidence that the model is essentially Gaussian, implying that the exponent in (1.2b) is $\lambda_\perp=2$. Recall that (2.14) is not exactly the same as (2.10), but the difference is insignificant, as discussed in Section 2.

A serious reason why, in our opinion, the argument of [15] cannot be regarded as a real proof or evidence that $\lambda_\perp=2$ really lies with the fact that practically the same or even better fit is provided by a non-Gaussian approximation of the form

$$G_\perp(k) \approx \chi_\perp \left(\frac{\tilde{a}}{\tilde{a}+\tilde{k}^2}\right)^{\lambda_\perp/2} \tag{3.2}$$

with $\tilde{k}^2 = (2\sin(k/2))^2$ for the transverse two-point correlation function in (2.8) with certain values of $\lambda_\perp < 2$. This approximation will be discussed in detail in Section 5. Here we only note that it is consistent with the modified Gaussian form at $\tilde{a}=m^2$ and $\lambda_\perp=2$, as well as with the general power-law asymptotic $ak^{-\lambda_\perp}$ at $h \to 0$ under an appropriate choice of $\tilde{a}=\tilde{a}(h)$. We have considered $\tilde{a}$ as the only fit parameter at a fixed exponent $\lambda_\perp=1.955$, consistent with the estimation for $n=4$ in [17]. The $\chi^2/$d.o.f. value of the

resulting $D_\perp(\tau)$ fit for the $\mathcal{O}(4)$ model at $L=128$ is 0.23. It is smaller than the value 0.4 of the Gaussian fit to (2.10) and even smaller than the value 0.36 of the fits to (2.14) and (2.13) (see Table 2). We have considered also the non-Gaussian fits with $\lambda_\perp=1.929$ for $n=2$ and $\lambda_\perp=1.972$ for $n=10$, as consistent with our estimation of the exponents in [16,19]. The non-Gaussian fits are shown by dotted lines in Fig. 2. As we can see, the Gaussian and non-Gaussian fit curves lie almost on top of each other. It means the analysis of the two-plane correlation functions hardly can give any serious evidence about the exponent $\lambda_\perp$.

It refers also to the spectral analysis of [15], where the transverse spectral function $\bar{A}(\omega)$ is defined as the solution of the integral equation

$$D_\perp(\tau)=\int_0^\infty \bar{A}(\omega)\bar{K}(\omega,\tau)d\omega, \tag{3.3}$$

with the kernel

$$\bar{K}(\omega,\tau)=\tanh\left(\frac{\omega}{2}\right)\frac{e^{-\omega\tau}+e^{-\omega(L-\tau)}}{1-e^{-\omega L}}. \tag{3.4}$$

According to [15], the solution is $\bar{A}(\omega)\approx\chi_\perp\delta(\omega-m)$. Numerically we never get the delta function, so that practically the spectrum consists of a sharp peak at $\omega=m$. In fact, $\bar{A}(\omega)\approx\chi_\perp\delta(\omega-m)$ means only that $D_\perp(\tau)\approx\chi_\perp\bar{K}(m,\tau)$ holds as a good approximation. According to the discussed here consistency of different fits, the latter is possible if the small-k asymptotic of $G_\perp(k)$ is given either by (2.11), or by (2.16), or by (3.2) with appropriate value of $\lambda_\perp<2$. Thus, no clear conclusion concerning $\lambda_\perp$ can be drawn here.

In fact, we need a direct estimation of the exponents, as in our papers [16–19], to judge seriously whether or not the asymptotic behavior of correlation functions and related quantities are Gaussian. Our estimation suggests that these are non-Gaussian.

Deviations of the simulated data points from the lower fit curves in Fig. 2 are practically the same for $\lambda_\perp=2$ and $\lambda_\perp=1.972$ in (3.2) (solid and dotted lines). Hence, if these deviations are not caused mainly by correlated and larger than usually statistical fluctuations, then one has to conclude that corrections to the form (3.2) are relevant in this case.

4　Universal ratios

The ratio bM^2/a^2, composed of the amplitudes a, b and magnetization $M=M(+0)$ in (1.2a)-(1.2c), is universal according to [20]. The ratio BM^2/A^2, where A and B are the corresponding amplitudes of the real-space correlation functions, can be easily related to bM^2/a^2. In the thermodynamic limit $L\to\infty$ for large $x=|\mathbf{x}|$ we have

$$\tilde{G}_j(\mathbf{x})=\tilde{G}_j(x)=\frac{1}{x}\frac{1}{2\pi^2}\int_0^\infty f(k)kG_j^{as}(k)\sin(kx)dk \tag{4.1}$$

in three dimensions, where $G_j^{as}(k)$ is an asymptotic approximation of $G_j(k)$, which is accurate for small k and decays smoothly for large k, and $f(k)$ is the cut-off function, which we choose as

$$f(k) = \frac{1}{1+(k/\Lambda)^4},$$

(4.2)

where Λ is a constant. This result is obtained by subtracting the constant contribution from (2.3), provided by $\mathbf{k}=0$, and replacing the remaining sum over $\mathbf{k}$ by the corresponding integral, taking into account that the correlation functions are asymptotically (at $x\to\infty$ or $k\to0$) isotropic in the thermodynamic limit. Here we use a smooth cut-off in the $\mathbf{k}$-space, which can be chosen quite arbitrary (however, ensuring the convergence of the integral), since only the small-k contribution is relevant for the large-x behavior.

As everywhere in this paper, $j=1$ can be replaced with "∥" and $j\geq2$ — with "⊥". The asymptotic of $\tilde{G}_\perp(x) = Ax^{\lambda_\perp-3}$ at $x\to\infty$, corresponding to $G_\perp(k)=ak^{-\lambda_\perp}$ at $k\to0$, as well as $\tilde{G}_\parallel(x)=Bx^{\lambda_\parallel-3}$ at $x\to\infty$, corresponding to $G_\parallel(k)=bk^{-\lambda_\parallel}$ at $k\to0$, can be easily calculated from (4.1), using the known relation [26,27]

$$\int_0^\infty k^{\alpha-1}f(k)\sin(kx)dk \sim x^{-\alpha}f(0)\Gamma(\alpha)\sin\left(\frac{\pi\alpha}{2}\right)$$

(4.3)

for $\alpha>0$ (the Erdélyi Lemma [26] applied to our particular case). It yields

$$\frac{bM^2}{a^2} = \frac{BM^2}{A^2}\frac{1}{2\pi^2}\frac{\Gamma^2(\eta^*)\sin^2\left(\frac{\pi}{2}\eta^*\right)}{\Gamma(1+2\eta^*)\sin\left(\frac{\pi}{2}(1+2\eta^*)\right)}$$

(4.4)

for $\eta^*=2-\lambda_\perp>0$ and $\lambda_\parallel=2\lambda_\perp-3$, corresponding to the relations of the GFD theory at $d=3$ [20]. The ratio bM^2/a^2 and, consequently, also BM^2/A^2 are universal in this theory. The standard-theoretical case $\eta^*=0$ is recovered at $\eta^*\to0$ in (4.4), as it can be checked by direct calculations. In this case, the usage of (4.3) at $\alpha=0$ is avoided, applying the known relation between the $1/(k^2+m^2)$ asymptotic (at small k and m in the thermodynamic limit) in $\mathbf{k}$-space and the $e^{-mx}/(4\pi x)$ asymptotic (at large x and small m in the thermodynamic limit) in $\mathbf{x}$-space and taking the limit $m\to0$. Thus, we obtain

$$\left(\frac{bM^2}{a^2}\right)_{st} = \frac{1}{8}\left(\frac{BM^2}{A^2}\right)_{st},$$

(4.5)

where the subscript "st" indicates that the quantity is calculated within the standard theory.

One of the cornerstones of the standard theory is the Patashinski-Pokrovski (PP) relation (see, e.g., [15] and references therein)

$$\tilde{G}_\parallel(\mathbf{x}) = \frac{n-1}{2M^2}\tilde{G}_\perp^2(\mathbf{x}).$$

(4.6)

It is supposed that (4.6) holds in the ordered phase in the thermodynamic limit for large distances, i.e., **x** can be replaced by $x = |\mathbf{x}|$ here. According to (4.6) and (4.5), we have

$$\left(\frac{BM^2}{A^2}\right)_{st} = \frac{n-1}{2}, \tag{4.7a}$$

$$\left(\frac{bM^2}{a^2}\right)_{st} = \frac{n-1}{16}. \tag{4.7b}$$

It turns out that these amplitude ratios can be precisely calculated in the standard theory, and they appear to be universal, as predicted by the GFD theory. The accuracy of the standard theory can be checked by comparing (4.7a)-(4.7b) with Monte Carlo estimates.

According to the relation $\lambda_\parallel = 2\lambda_\perp - d$, which holds in the GFD theory [20] and also in the standard theory (where $\lambda_\perp = 2$ and $\lambda_\parallel = 4 - d$), in 3D case we have

$$\frac{bM^2}{a^2} = \lim_{k \to 0} R(k), \tag{4.8}$$

where the quantity

$$R(k) = \frac{M^2 G_\parallel(k)}{k^3 G_\perp^2(k)} \tag{4.9}$$

is calculated in the thermodynamic limit at $h = +0$. In order to estimate $R(0)$ in this limit, we consider appropriate range of k values, i.e., $k > k^*$, for small fields h and large system sizes L, where the finite-size effects are very small or practically negligible and the finite-h effects are also small. Then, we extrapolate the $R(k)$ plots to $k = 0$ at several h values to find the required asymptotic value of $R(0) = bM^2/a^2$. Such analysis has been already performed in [19] for the $\mathcal{O}(4)$ model at $\beta = 1.1$ and $\beta = 1.2$, with an aim to test the universality of bM^2/a^2 predicted in [20]. It has been confirmed, providing an estimate $bM^2/a^2 = 0.17 \pm 0.01$ valid for both values of β. Now we can see from (4.7b) that this estimate is slightly smaller than the standard-theoretical value $3/16 = 0.1875$.

Here we consider the cases $n = 2$ and $n = 10$. The choice of the k-interval for the $\mathcal{O}(2)$ model is illustrated in Fig. 3, where we can see that the finite-size and finite-h effects are very small for $G_\perp(k)$ if $k \geq k_9$, and these are small also for $G_\parallel(k)$ if $k \geq k_{20}$ with $k_\ell = 2\pi\ell/512$. Hence, the region $k \geq k_{20}$ is appropriate for the estimation of $R(k)$. Similarly, we have found that the region $k \geq k_{15}$ with $k_\ell = 2\pi\ell/350$ is appropriate for our analysis at $n = 10$. The plots similar to those in Fig. 3 for $n = 10$ are given in [19] (see Figs. 1 and 2 there).

The local slopes of plots in Fig. 3 are the effective exponents, which are meaningful in the discussed here ranges, $k > k_\perp^* = k_9$ for $G_\perp(k)$ and $k > k_\parallel^* = k_{20}$ for $G_\parallel(k)$, where the curves at small h practically merge. The effective exponents, evaluated from the fits within $[k, 2k]$, are shown as functions of k in Fig. 4. One can judge from the behavior of the transverse effective exponent (upper curves) within $k > k_\perp^*$ that the asymptotic exponent $\lambda_\perp$ is close to the standard-theoretical value 2. To the contrary, plots of the longitudinal effective exponent (lower curves) deviate below the standard-theoretical value 1. For a detailed
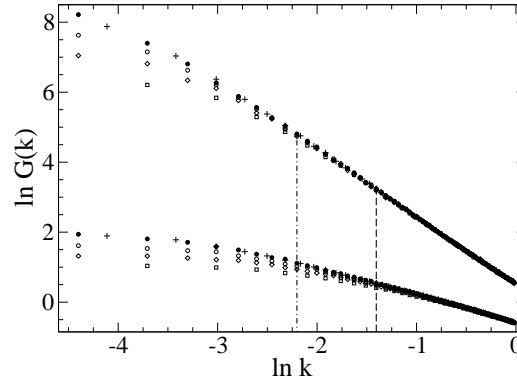
Figure 3: Log-log plots of the transverse (top) and the longitudinal (bottom) Fourier-transformed two-point correlation functions in the $\mathcal{O}(2)$ model (shown for $k<1$ at $\beta=0.55$) at $h=h_{\min}=0.00021875$ and $L=512$ (solid circles), $h=h_{\min}$ and $L=384$ (pluses), $h=2h_{\min}$ and $L=512$ (empty circles), $h=4h_{\min}$ and $L=512$ (diamonds), $h=8h_{\min}$ and $L=256$ (squares). The vertical dot-dashed and dashed lines indicates the lower borders of the k intervals where the finite-size and finite-h effects are small for $G_{\perp}(k)$ and $G_{\parallel}(k)$, respectively.
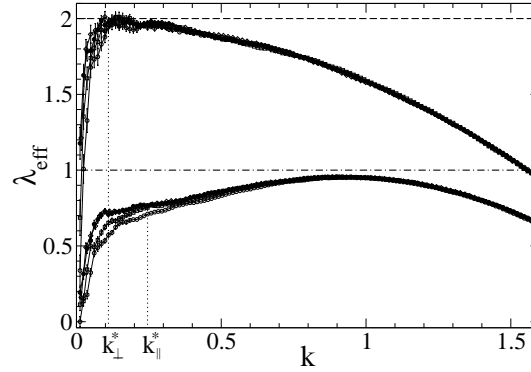

Figure 4: Transverse (top) and longitudinal (bottom) effective exponents of the $\mathcal{O}(2)$ model at $h=h_{\min}=0.00021875$ and $L=512$ (solid circles), $h=h_{\min}$ and $L=384$ (diamonds), $h=2h_{\min}$ and $L=512$ (squares), $h=4h_{\min}$ and $L=512$ (empty circles). The vertical dotted lines indicate the lower borders of the k intervals ($k_{\perp}^{*}$ in the transverse case and $k_{\parallel}^{*}$ in the longitudinal case), where the plots merge for small h values.

analysis of these plots see [18], where an estimate $\lambda_{\parallel}=0.69\pm0.10$ is obtained, assuming corrections to scaling of the standard theory. We cannot rule out a possibility that this effective exponent converges to 1, if appropriately estimated at $k<k_{20}$ (simulations for smaller h and larger L values would be necessary in this case), although the current data give no evidence for such a possible scenario. The effective transverse and longitudinal exponents show a remarkable h-dependence and crossover effects within $k<k_{\perp}^{*}$ and $k<k_{\parallel}^{*}$, respectively. These, however, are trivial crossovers, which always occur for small enough wave vectors at any finite h value, i.e., crossovers from the power-law behavior to the $\propto 1/(a+k^2)$ behavior. The latter one always takes place at a finite h in vicinity of $k=0$, where the correlation functions can be expanded in powers of k^2. In fact, the effective
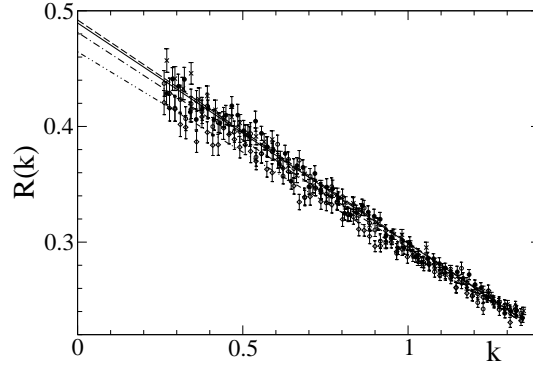
Figure 5: The ratio $R(k)$ (4.9) in the $\mathcal{O}(10)$ model at $\beta=3$. The results for $h=h_{\min}=0.00021875$ and $L=350$ (solid circles), $h=h_{\min}$ and $L=256$ (exes), $h=2h_{\min}$ and $L=384$ (empty circles), as well as for $h=4h_{\min}$ and $L=384$ (diamonds) are presented. The respective linear fits are shown by solid, dashed, dot-dashed and dot-dot-dashed lines. The fit interval is $k_{15} \leq k \leq k_{75}$ with $k_\ell = 2\pi\ell/350$ for $L=350$ and similar in other cases.

exponents tend to zero at $k \to 0$ because of this effect. Hence, this trivial behavior gives no indication that some non-trivial crossover, probably, takes place.

We will start our estimation of $R(0)$ with $n=10$, since the results are more precise and convincing in this case. According to the corrections to scaling of the standard theory, the correlation functions are expanded in powers of k^{4-d} and k^{d-2} [1,5], i.e., in powers of k at small wave vectors in three dimensions. It means that the ratio $R(k)$ is expected to be linear function of k at $k \to 0$. We indeed observe a very good linearity for the $\mathcal{O}(10)$ model within $k_{15} \leq k \leq k_{75}$ ($k_\ell = 2\pi\ell/350$), as it can be seen from Fig. 5, where the fit results for this or very similar intervals are shown at different fields h and lattice sizes L. For the smallest h value $h=h_{\min}=0.00021875$, the linear fits give $R(0)=0.4895(27), 0.4920(27), 0.4936(26)$ and $0.5021(28)$ at $L=350, 256, 192$ and 128, respectively. Hence we can judge that the finite-size effects are practically negligible at $L=350$. The results for $h=2h_{\min}$ and $h=4h_{\min}$ at $L=384$ are $R(0)=0.4814(27)$ and $R(0)=0.4646(28)$, respectively.

To control the linearity, we have evaluated the slope of the $R(k)$ plot for the smallest-h data at $L=350$ by fitting these data within the interval $[k, k+k_{15}]$ and have plotted the result as a function of k in Fig. 6. At $k=0$, it corresponds to the average slope within $[0, k_{15}]$, i.e., within the gap in Fig. 5, where the data are absent. It is related to the increment of $R(k)$ within this gap. In fact, if the standard-theoretical asymptotic value $9/16=0.5625$ is correct, then this increment has to be more than twice larger than that of the linear extrapolation in Fig. 5. We find that the average slope within $[0, k_{15}]$ has to be about -0.43 in this case. This value is indicated by the lower dot-dot-dashed line in Fig. 6. The slopes evaluated from the data in Fig. 5 correspond to $k \leq k_{60}$ in Fig. 6, where k_{60} is indicated by the vertical dotted line. Although the data contain a remarkable statistical noise (a correlated noise), one can judge that these slopes fluctuate around the average value $-0.1906(26)$ (the dot-dashed line) for the range $[k_{15}, k_{75}]$ in Fig. 5 rather than tend to -0.43 (the dot-dot-dashed line). It justifies the linear fit as a reasonable approximation,
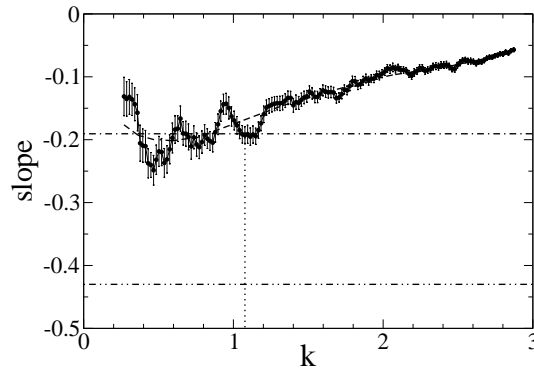
Figure 6: The slope of the $R(k)$ plot depending on k for the $\mathcal{O}(10)$ model, evaluated from the fits of the smallest-h data at $L=350$ within $[k,k+k_{15}]$. The estimates extracted from the data within the k range in Fig. 5 correspond to $k \leq k_{60}$. The value k_{60} is indicated by a vertical dotted line. The upper dot-dashed line indicates the average slope $-0.1906(26)$ in Fig. 5. The lower dot-dot-dashed line indicates the expected average slope within $[0,k_{15}]$, which is about -0.43, if the standard-theoretical value $R(0) = 9/16$ is correct. The dashed curve is a guide to eye.
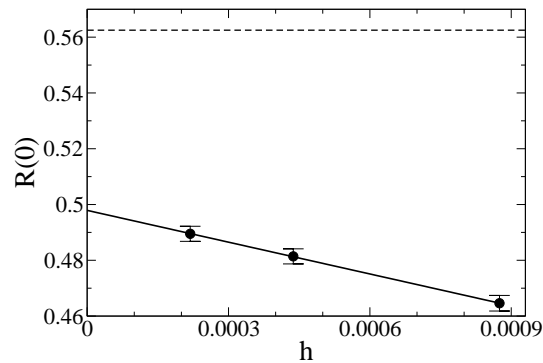

Figure 7: The values of $R(0)$ (solid circles), evaluated from the fits in Fig. 5 depending on the external field h, taking the largest size L for each h. The linear fit gives an estimate $R(0) = 0.4979(33)$ for $h = +0$. The standard-theoretical value $9/16 = 0.5625$ is indicated by dashed line.

although some nonlinearity could be present, if the slope for the interval $[k,k+k_{15}]$ is slightly varied within $k < k_{60}$, e.g., as shown by the dashed curve in Fig. 6.

In Fig. 7, the $R(0)$ estimates for the largest sizes are shown depending on h. The three data points almost precisely fit on a straight line, which gives the asymptotic estimate $R(0) = 0.4979(33)$ for $h = +0$. This fit is plausible from the point of view that the h-dependence is, indeed, expected to be smooth (analytic) for a fixed interval of nonzero k values, where $R(k)$ has been calculated. Note, however, that the indicated here error bars ± 0.0033 include only the statistical error. A systematic error can arise from a weak nonlinearity of the plot and also from finite-size effects, which seem to be smaller than the statistical error bars in this case. Since the possible non-linearity is not well controlled having only three data points, we have set remarkably larger error bars ± 0.01 for our final
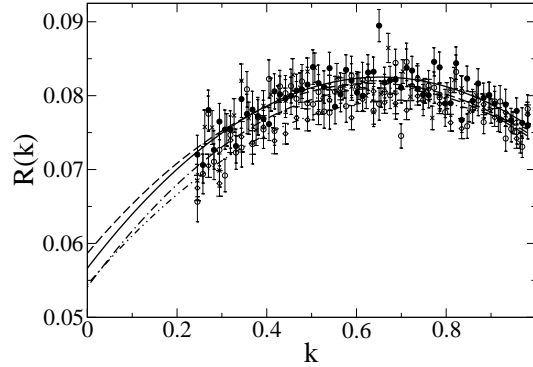
Figure 8: The ratio $R(k)$ (4.9) in the $\mathcal{O}(2)$ model at $\beta = 0.55$. The results for $h = 2h_{\min} = 0.0004375$ and $L = 512$ (solid circles), $h = 2h_{\min}$ and $L = 384$ (exes), $h = 4h_{\min}$ and $L = 512$ (empty circles), and for $h = 8h_{\min}$ and $L = 256$ (diamonds) are presented. The respective quadratic fits are shown by solid, dashed, dot-dashed and dot-dot-dashed lines and yield $R(0) = 0.0566(22), 0.0587(26), 0.0541(25)$ and $0.0544(23)$. The fit interval is $k_{20} \leq k \leq k_{80}$ with $k_\ell = 2\pi\ell/512$ for $L = 512$ and similar in other cases.

estimate $R(0) = bM^2/a^2 = 0.498 \pm 0.010$. This estimate shows a small, but very remarkable as compared to the error bars, deviation from the standard-theoretical value (4.7b) $bM^2/a^2 = 9/16 = 0.5625$, indicated in Fig. 7 by a dashed line.

A similar estimation is performed here for the $\mathcal{O}(2)$ model, with an essential difference that the $R(k)$ plots appear to be rather non-linear, well fit to a parabola instead of a straight line. Besides, in this case we have used the data for larger fields $h = 2h_{\min}$, $h = 4h_{\min}$ and $h = 8h_{\min}$, since the agreement between the results for different lattice sizes at $h = h_{\min}$ was not as good (although the estimate $R(0) = 0.0590(24)$ at the largest size $L = 512$ and $h = h_{\min}$, probably, is good). In such a way, based on the fits shown in Fig. 8, we have made a rough estimation $R(0) = bM^2/a^2 = 0.06 \pm 0.01$ for the $\mathcal{O}(2)$ model. It agrees within the error bars with the standard-theoretical value $1/16 = 0.0625$.

5   Analytic approximations for $G_\perp(k)$ and $G_\parallel(k)$

Let us now consider the approximation (3.2) in more detail. This approximation does not uniquely follow from the theory in [20], since the letter refers mainly to the case $h = +0$ in the thermodynamic limit. However, this approximation for non-zero h together with an analogous one for the longitudinal correlation function, i.e.,

$$G_\perp(k) \approx \chi_\perp \left(\frac{\tilde{a}(h)}{\tilde{a}(h) + \tilde{k}^2} \right)^{\lambda_\perp/2}, \tag{5.1a}$$

$$G_\parallel(k) \approx \chi_\parallel \left(\frac{\tilde{b}(h)}{\tilde{b}(h) + \tilde{k}^2} \right)^{\lambda_\parallel/2}, \tag{5.1b}$$

where $\tilde{k}^2 = (2\sin(k/2))^2$, have the expected properties under appropriate choice of parameters $\tilde{a} = \tilde{a}(h)$ and $\tilde{b} = \tilde{b}(h)$. The actual choice of $\tilde{k}^2$ ensures the periodicity $G_\perp(k + 2\pi) =$

$G_\perp(k)$ and $G_\parallel(k+2\pi)=G_\parallel(k)$ and, at the same time, $\tilde{k}^2\to k^2$ at $k\to 0$. The formulas (5.1a) and (5.1b) ensure that the correlation functions can be expanded in powers of k^2 in vicinity of $k=0$ for any nonzero h. At the same time they ensure the power-law asymptotic $G_\perp(k)=ak^{-\lambda_\perp}$ and $G_\parallel(k)=bk^{-\lambda_\parallel}$ at $h\to 0$ provided that $\tilde{a}(h)\sim\tilde{b}(h)\sim h^{2/\lambda_\perp}$ holds at $h\to 0$, taking into account the relations $\chi_\perp=M(h)/(\beta h)$ and $\chi_\parallel\sim h^{-\lambda_\parallel/\lambda_\perp}$. The latter one is true at $h\to 0$ according to Eq. (9.25) in [20]. This behavior of $\tilde{a}(h)$ and $\tilde{b}(h)$ implies that $\xi_\perp(h)\sim\xi_\parallel(h)\sim h^{-1/\lambda_\perp}$ holds for small h, where $\xi_\perp$ and $\xi_\parallel$ are the transverse and the longitudinal correlation lengths. Similar conclusion follows from the PP relation (4.6), i.e., $\xi_\perp/\xi_\parallel=2$. However, according to (5.1a)-(5.1b), the ratio $\xi_\perp/\xi_\parallel$ is expected to be a constant at $h\to 0$, but not necessarily two.

Apparently, Eqs. (5.1a)-(5.1b) represent the simplest possible form having the above discussed properties. Therefore, this form might be a very reasonable first approximation for small k, at least. Recall that the simulated quantities $G_\perp(k)$ and $G_\parallel(k)$ are the correlation functions in the $\langle 100\rangle$ crystallographic direction. However, the expressions in the right hand side of (5.1a) and (5.1b) might be generally meaningful approximations for $G_\perp(\mathbf{k})$ and $G_\parallel(\mathbf{k})$ with $\tilde{k}^2$ given by (2.12).

The Gaussian transverse correlation function (2.9) is interpreted as one corresponding to a particle with mass m in the quantum field theory. The true correlation function can be related to particles with certain mass spectrum $A(\omega)$ via

$$G_\perp(\mathbf{k})=\int_\omega A(\omega)\mathcal{K}(\omega,\mathbf{k})d\omega, \tag{5.2}$$

where $\mathcal{K}(\omega,\mathbf{k})$ can be an appropriately modified Gaussian propagator, like (2.11) or (2.16), with $m=\omega$. If the true correlation function is just $\mathcal{K}(m,\mathbf{k})$, then we have $A(\omega)=\delta(m-\omega)$. Our fits suggest that the approximation (5.1a) is valid with slightly smaller than 2 value of the exponent $\lambda_\perp$. In this case, the spectral function could also exist. In particular, small deviations from the Gaussian form might imply that $A(\omega)$ has a sharp maximum at $\omega=m$, the maximum value being finite. The question about the existence of such a spectral representation is not quite trivial and requires a further investigation. It refers also to possible spectral representations of the longitudinal correlation function.

In the following, we have considered $\tilde{a}(h)$ and $\tilde{b}(h)$, as well as the exponents $\lambda_\perp$ and $\lambda_\parallel$ as fit parameters in (5.1a) and (5.1b). In such a way, (5.1a) is consistent also with the standard theory if $\lambda_\perp=2$ holds within the error bars. We have found that (5.1a) fairly well fits our data for $\mathcal{O}(n)$ models at various parameters within the whole range of the wave vector magnitude $k\le\pi$. The fit results are collected in Table 4. Those for a narrower k interval $k<0.55$ are presented in Table 5. The results of fits to (5.1b) for the longitudinal two-point correlation function are presented in Table 6. In this case, the data cannot be well fit within $k\le\pi$. It is also not always possible for $k<0.55$, but the fits improve significantly (on average) for a narrower interval $k<0.28$. For the intervals $k<0.55$ and $k<0.28$, fits to the asymptotic form, where $\tilde{k}^2$ is replaced by k^2 in (5.1a) and (5.1b), have a similar quality than those presented in Tables 5 and 6. The results are also similar.

Table 4: Parameters used in (5.1a), $\tilde{a}(h)$ and $\lambda_\perp$ being evaluated from fits within $k \leq \pi$.

n	β	$10^4 h$	L	$\chi_\perp$	$10^4 \tilde{a}(h)$	$\lambda_\perp$	χ^2/d.o.f.
2	0.55	2.1875	512	5254.762(75)	2.624(14)	1.9696(11)	1.16
2	0.55	4.375	512	2630.392(25)	5.364(33)	1.9723(15)	1.18
2	0.55	8.75	512	1317.3967(86)	10.828(62)	1.9722(15)	1.29
4	1.1	3.125	350	1422.831(40)	5.354(26)	1.9776(11)	1.10
4	1.1	4.375	350	1018.173(24)	7.527(36)	1.9783(12)	1.36
4	1.2	4.375	350	1075.028(19)	6.709(33)	1.9840(12)	1.31
10	3	2.1875	350	719.464(24)	4.331(18)	1.99225(98)	1.22
10	3	4.375	384	361.3551(75)	8.676(34)	1.9931(10)	0.91
10	3	8.75	384	181.8192(29)	17.215(57)	1.99227(95)	1.17

Table 5: Parameters used in (5.1a), $\tilde{a}(h)$ and $\lambda_\perp$ being evaluated from fits within $k < 0.55$.

n	β	$10^4 h$	L	$\chi_\perp$	$10^4 \tilde{a}(h)$	$\lambda_\perp$	χ^2/d.o.f.
2	0.55	2.1875	512	5254.762(75)	2.805(47)	1.9897(56)	0.76
2	0.55	4.375	512	2630.392(25)	5.866(84)	2.0037(53)	0.61
2	0.55	8.75	512	1317.3967(86)	11.59(20)	1.9996(72)	1.32
4	1.1	3.125	350	1422.831(40)	5.500(73)	1.9857(49)	1.24
4	1.1	4.375	350	1018.173(24)	7.90(11)	1.9959(58)	1.10
4	1.2	4.375	350	1075.028(19)	7.032(84)	2.0011(46)	1.01
10	3	2.1875	350	719.464(24)	4.333(47)	1.9918(39)	1.35
10	3	4.375	384	361.3551(75)	8.766(98)	1.9973(45)	0.61
10	3	8.75	384	181.8192(29)	17.39(20)	1.9965(54)	1.37

If we consider such fits as a method of estimation of the exponents $\lambda_\perp$ and $\lambda_\parallel$, then it has certain advantage as compared to the estimations in [18, 19], i.e., it is not necessary to discard the smallest k values in order to ensure the smallness of the finite-h effects. However, a disadvantage is that no corrections to scaling are included in (5.1a)-(5.1b). Therefore, the values reported in [16–19] are preferable as asymptotic estimates.

The $\lambda_\perp$ values in Table 4 show quite negligible finite-h effects and small, but very remarkable as compared to the statistical error bars, deviations below the standard-theoretical value 2. These deviations, obviously, are not caused by finite-size effects, since the results for remarkably smaller lattice sizes are practically the same. Namely, at the smallest h values we have $\lambda_\perp = 1.9719(12)$ for $n = 2$ and $L = 256$, $\lambda_\perp = 1.9796(12)$ for $n = 4$ and $L = 128$, and $\lambda_\perp = 1.9933(12)$ for $n = 10$ and $L = 192$. However, the estimates in Table 4 could have some systematic errors because of too large wave vectors included in the fits. In this case, the fits over a narrower range $k < 0.55$ (see Table 5) are more appropriate. The exponents $\lambda_\perp$ in Table 5 slightly depend on the field h. Comparing the values at two smallest fields in each of the cases $n = 2$, $n = 4$ and $n = 10$, we can see some tendency of decreasing with decreasing of h, in such a way that the asymptotic values at $h = +0$

Table 6: Parameters used in (5.1b), $\tilde{b}(h)$ and $\lambda_\parallel$ being evaluated from fits within $k < k_{\max}$.

n	β	$10^4 h$	L	$k_{\max}$	$\chi_\parallel$	$10^2 \tilde{b}(h)$	$\lambda_\parallel$	$\chi^2/\text{d.o.f.}$
2	0.55	2.1875	512	0.28	7.62(25)	0.110(16)	0.737(12)	1.84
2	0.55	2.1875	512	0.55	7.62(25)	0.126(14)	0.7659(47)	1.81
2	0.55	4.375	512	0.28	5.29(15)	0.230(38)	0.690(19)	1.41
2	0.55	4.375	512	0.55	5.29(15)	0.297(35)	0.7545(81)	2.48
2	0.55	8.75	512	0.28	3.764(95)	0.71(13)	0.756(36)	0.88
2	0.55	8.75	512	0.55	3.764(95)	0.717(85)	0.758(12)	0.82
4	1.1	3.125	350	0.28	7.41(20)	0.277(36)	0.872(22)	1.51
4	1.1	3.125	350	0.55	7.41(20)	0.378(33)	0.9799(94)	3.27
4	1.1	4.375	350	0.28	6.36(17)	0.403(59)	0.892(29)	1.18
4	1.1	4.375	350	0.55	6.36(17)	0.512(48)	0.983(12)	1.86
4	1.2	4.375	350	0.28	4.27(14)	0.356(57)	0.878(28)	0.82
4	1.2	4.375	350	0.55	4.27(14)	0.431(48)	0.945(12)	1.58
10	3	2.1875	350	0.28	4.18(20)	0.212(44)	0.947(34)	1.61
10	3	2.1875	350	0.55	4.18(20)	0.289(40)	1.061(14)	2.24
10	3	4.375	384	0.28	2.624(98)	0.68(14)	1.043(62)	0.90
10	3	4.375	384	0.55	2.624(98)	0.79(10)	1.115(22)	0.86
10	3	8.75	384	0.28	1.920(72)	1.16(32)	1.026(96)	0.72
10	3	8.75	384	0.55	1.920(72)	1.43(22)	1.144(35)	0.74

could be quite similar to our earlier estimates, at least for $n = 4$ and $n = 10$. Recall that the values 1.955 ± 0.020 and $1.960(10)$ for $n = 4$ and $1.9723(90)$ for $n = 10$ have been reported in [17,19]. The longitudinal exponent $\lambda_\parallel = 2\lambda_\perp - d$, calculated from these asymptotic estimates, is consistent with $\lambda_\parallel$ for relatively small k values ($k_{\max} = 0.28$) at the smallest fields h in Table 6.

For the $\mathcal{O}(2)$ model, the agreement between $\lambda_\perp = 1.929(21)$, obtained in [16] from (1.2a) via scaling relation $\rho = (d/\lambda_\perp) - 1$ [20], and the smallest-h estimate $\lambda_\perp = 1.9897(56)$ in Table 5 is remarkably worse. The exponent $\lambda_\parallel = 0.737(12)$ in Table 6 (at minimal h and $k_{\max} = 0.28$) is somewhat smaller than the value $0.858(42)$, calculated from the scaling relation $\lambda_\parallel = 2\lambda_\perp - d$ [20] with $\lambda_\perp = 1.929(21)$, although it agrees well with the direct estimation $\lambda_\parallel = 0.69 \pm 0.10$ in [18]. The discrepancies indicate that corrections to scaling, including non-trivial ones of the GFD theory (discussed in [18,19]), which have not been taken into account in the fitting procedures, are larger for the $\mathcal{O}(2)$ model as compared to the $\mathcal{O}(4)$ and $\mathcal{O}(10)$ models.

In Figs. 9 and 10, some of our fit curves at $h = 0.0004375$ are shown, which are relatively good, especially for $n = 4$ and $n = 10$. These are fits to the asymptotic form of (5.1a) and (5.1b) for small k values, where $\tilde{k}^2$ is replaced by k^2. The fit curves for $\tilde{k}^2 = (2\sin(k/2))^2$ look practically the same. The asymptotic case is shown here, since just these fits are used in our further analysis in Section 6.
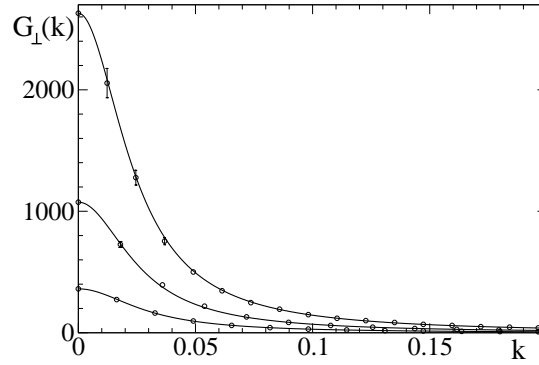
Figure 9: The transverse two-point correlation function $G_\perp(k)$ at the value of external field $h = 0.0004375$. The results for the $\mathcal{O}(2)$ model at $\beta = 0.55$ and $L = 512$ (top), $\mathcal{O}(4)$ model at $\beta = 1.2$ and $L = 350$ (middle), and $\mathcal{O}(10)$ model at $\beta = 3$ and $L = 384$ (bottom) are presented. The simulated data points are shown by circles. The error bars are indicated, where these are larger than the symbol size. Curves represent the asymptotic form of (5.1a) with $\tilde{k}^2 = k^2$, parameters $\tilde{a}(h)$ and $\lambda_\perp$ being evaluated from the fits within $k < 0.55$.
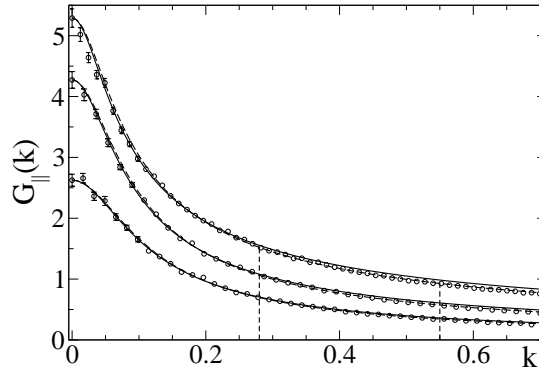

Figure 10: The longitudinal two-point correlation function $G_\parallel(k)$ for the $\mathcal{O}(2)$ model (top), $\mathcal{O}(4)$ model (middle), and $\mathcal{O}(10)$ model (bottom) at the same parameters as $G_\perp(k)$ in Fig. 9. The simulated data points are shown by circles, the error bars being indicated, where these exceed the symbol size. The fits to the asymptotic form of (5.1b) with $\tilde{k}^2 = k^2$ are shown by solid and dashed curves for the fit ranges $k < 0.28$ and $k < 0.55$, respectively. The upper values of the fit intervals are indicated by vertical dashed lines.

6 Test of the Patashinski-Pokrovski relation

The fit curves for the $\mathcal{O}(4)$ and $\mathcal{O}(10)$ models in Figs. 9 and 10 provide good approximations in the thermodynamic limit at the given parameters and small k values, and these approximation functions decay smoothly for large k. Therefore we have used them for $G_j^{as}(k)$ in Eq. (4.1). It allowed us to test the PP relation (4.6) for large distances x via (4.1) and (4.2). In the case of a finite lattice, the wave vectors belong to a cube with $-\pi \le k_x \le \pi$, $-\pi \le k_y \le \pi$, $-\pi \le k_z \le \pi$. Therefore a reasonable choice of the cut-off parameter is $\Lambda = \pi$. The precise value of Λ, however, is not important, since the result for $\tilde{G}_j(x)$ is insensitive
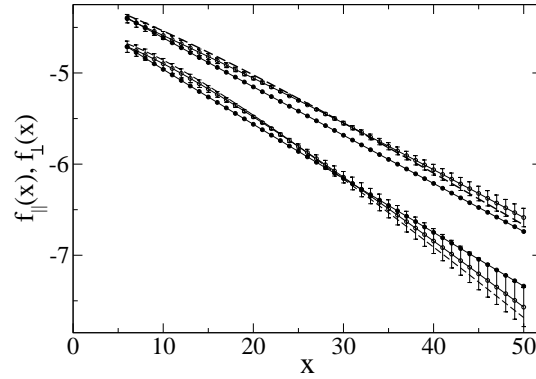
Figure 11: The functions $f_\perp(x)$ (6.1a) and $f_\parallel(x)$ (6.1b) for the $\mathcal{O}(4)$ (upper curves) and $\mathcal{O}(10)$ (lower curves) models, evaluated from (4.1) (replacing i with $\perp$ or $\parallel$) and (4.2) with $\Lambda=\pi$, using the fit functions $G_\perp(k)$ and $G_\parallel(k)$ in Figs. 9 and 10. The solid circles correspond to $f_\perp(x)$, the error bars being smaller than the symbol size. The empty circles with error bars represent $f_\parallel(x)$, evaluated using the fit interval $k<0.28$ in Fig. 10, the results for $k<0.55$ being indicated by dashed curves. The PP relation (4.6) implies $f_\perp(x)=f_\parallel(x)$.

to the variation of Λ at large enough x. We calculate functions $f_\perp(x)$ and $f_\parallel(x)$ given by

$$f_\perp(x)=2\ln(x\tilde{G}_\perp(x))+\ln\left(\frac{n-1}{2M^2}\right), \tag{6.1a}$$

$$f_\parallel(x)=\ln\left(x^2\tilde{G}_\parallel(x)\right), \tag{6.1b}$$

which have to be equal if the PP relation holds. In the Gaussian approximation (2.9), we have $\tilde{G}_\perp(x)\propto e^{-mx}/x$ at $x\to\infty$, implying the linearity of these functions at large x.

The magnetization M for the actual parameters are taken from [17, 19]. We have considered the distances $x\geq 6$, as in this case the $f_\parallel(x)$ curves at $\Lambda=\pi$ and $\Lambda=\pi/2$ lie practically on top of each other. The function $f_\perp(x)$ is even much less influenced by the change of Λ. The used here fits in Fig. 9 are perfect, whereas those in Fig. 10 show some systematic variations depending on the fit interval. The fits over $k<0.28$ are better for small k, therefore they could provide a better approximation of $f_\parallel(x)$ for large x, although the fits over a wider interval $k<0.55$ look better on average. We have compared the results in both cases to judge about the magnitude of systematic errors. The resulting curves of $f_\perp(x)$ and $f_\parallel(x)$ within $6\leq x\leq 50$ are shown in Fig. 11. The errors due to statistical and systematic uncertainties in the fit parameters increase significantly for $x>50$, therefore no larger distances are considered here. As we can judge from Fig. 11, the PP relation holds approximately (within 10% or 15% accuracy) in these examples at a finite external field $h=0.0004375$.

Another case, where the PP relation can be tested, is the large-x behavior in the thermodynamic limit at $h=+0$. It is closely related to the universal ratio test in Section 4. The PP relation states that (4.7a) must hold for the ratio BM^2/A^2. As it is shown in Section 4, this requirement is equivalent to (4.7b) for the ratio bM^2/a^2, if the transverse exponent is

$\lambda_\perp = 2$, as predicted by the standard theory. Tests in Section 4 show certain inconsistencies with (4.7b) (see Fig. 7) and, consequently, with the PP relation if $\lambda_\perp = 2$. Assuming that $\lambda_\perp = 2$ holds at $n = 10$, the ratio $BM^2/A^2 = 8bM^2/a^2 = 3.984 \pm 0.080$ (see Eq. (4.5)) appears to be somewhat smaller than the value 4.5 expected from the PP relation. One can use (4.4) to calculate BM^2/A^2 from bM^2/a^2 at our numerically estimated values of the exponent $\lambda_\perp < 2$. It leads to slightly (by $\sim 1\%$) smaller values of BM^2/A^2. Thus, we find that the PP relation holds approximately (within about 12% accuracy in our examples) in the thermodynamic limit for large $x \to \infty$ at $h = +0$.

7 Conclusions

In the current paper, we have considered the behavior of the longitudinal and transverse correlation functions and Goldstone mode singularities in $\mathcal{O}(n)$ models from different aspects compared to our earlier Monte Carlo studies [16–19]. Apart from the two-point correlation functions, here we have calculated the two-plane correlation functions, which are very important for the provided here discussions related to the recent work by Engels and Vogt [15]. We confirm the stated in [15] fact that the transverse two-plane correlation function of the $\mathcal{O}(4)$ model for lattice sizes about $L = 120$ and small external fields h is very well described by a Gaussian approximation with $\lambda_\perp = 2$ in (1.2b). However, we have shown in Section 3 that fits of not lower quality are provided by certain non-Gaussian approximation, where $\lambda_\perp < 2$. Thus, the behavior of the two-plane correlation functions does not imply that the $\mathcal{O}(4)$ model is essentially Gaussian with $\lambda_\perp = 2$. We have also tested the cases $n = 2, 4, 10$ for larger lattice sizes (e.g., $L = 350$ and $L = 512$), where not as good agreement with the Gaussian model has been observed.

The ratio bM^2/a^2 has been considered in Section 4, showing that its universality follows not only from the GFD theory [20], but also from the standard theory, yielding $bM^2/a^2 = (n-1)/16$. Our MC estimates of this ratio are 0.06 ± 0.01 for $n = 2$, 0.17 ± 0.01 for $n = 4$ and 0.498 ± 0.010 for $n = 10$. The latter estimate shows a very remarkable, as compared to the error bars, deviation from the standard-theoretical value $9/16 = 0.5625$. Our MC estimation in [16,17,19] points to small deviations from the standard-theoretical predictions in favor of the GFD theory. A clear evidence that the standard theory is not asymptotically exact (as one often claims) at large length scales has been provided in [18], showing that a self consistent (within the standard theory) estimation of the longitudinal exponent $\lambda_\parallel$ from MC data of the three-dimensional $\mathcal{O}(2)$ model at $\beta = 0.55 > \beta_c$ yields $\lambda_\parallel = 0.69 \pm 0.10$ in disagreement with the expected value $\lambda_\parallel = 1$. The current MC estimation of the ratio bM^2/a^2 provides one more such evidence. One has to note that the standard-theoretical exponent $\rho = 1/2$ in (1.2a) is apparently confirmed by the experimental data of [28]. However, in our opinion, the low quality of fits (i.e., evident systematic deviations of the data points from the fit curves) in Fig. 1 of [28] rises a question whether this exponent is just $1/2$ or, perhaps, slightly different from $1/2$.

In Section 5, we have proposed and tested certain analytic approximations for the

two-point correlation functions $G_\perp(k)$ and $G_\parallel(k)$ in $\langle 100 \rangle$ direction and also for $G_\perp(\mathbf{k})$ and $G_\parallel(\mathbf{k})$ at small $k = |\mathbf{k}|$, which are consistent with the expected behavior at $h = +0$ and are valid also at a finite external field h. We have found that these approximations (Eqs. (5.1a) and (5.1b)) fit reasonably well the simulation data for small k. Moreover, (5.1a) quite well tits the $G_\perp(k)$ data within the whole range $k \in [0,\pi]$. The exponents $\lambda_\perp$ and $\lambda_\parallel$ in (5.1a)-(5.1b) have been discussed as fit parameters, showing that these are comparable with our earlier estimates. In Section 6, we have used our analytic approximations to test the Patashinski-Pokrovski relation (4.6), and have found that it holds approximately within the accuracy of about 10% or 15% in the examples considered.

Acknowledgments

References

[1] I. D. Lawrie, Goldstone modes and coexistence in isotropic N-vector models, J. Phys. A, 14, 14 (1981), 2489–2502.
[2] I. D. Lawrie, Goldstone mode singularities in specific heats and non-ordering susceptibilities of isotropic systems, J. Phys. A, 18 (1985), 1141–1152.
[3] P. Hasenfratz and H. Leutwyler, Goldstone boson related finite size effects in field theory and critical phenomena with $\mathcal{O}(n)$ symmetry, Nucl. Phys., B343 (1990), 241–284.
[4] U. C. Täuber and F. Schwabl, Critical dynamics of the $\mathcal{O}(n)$-symmetric relaxational models below the transition temperature, Phys. Rev. B, 46 (1992), 3337–3361.
[5] L. Schäfer and H. Horner, Goldstone mode singularities and equation of state of an isotropic magnet, Z. Phys. B, 29 (1978), 251.
[6] R. Anishetty, R. Basu, N. D. Hari Dass and H. S. Sharatchandra, Infrared behaviour of systems with goldstone bosons, Int. J. Mod. Phys., A14 (1999), 3467–3496.
[7] N. Dupuis, Infrared behavior in systems with a broken continuous symmetry: classical $\mathcal{O}(N)$ model versus interacting bosons, Phys. Rev. E, 83 (2011), 031120.
[8] E. Brézin and D. J. Wallace, Critical behavior of a classical heisenberg ferromagnet with many degrees of freedom, Phys. Rev. B, 7 (1973), 1967–1974.
[9] D. J. Wallace and R. K. Zia, Singularities induced by Goldstone modes, Phys. Rev. B, 12 (1975), 5340–5342.
[10] D. R. Nelson, Coexistence-curve singularities in isotropic ferromagnets, Phys. Rev. B, 13 (1976), 2222–2230.
[11] E. Brézin and J. Zinn-Justin, Spontaneous breakdown of continuous symmetries near two dimensions, Phys. Rev. B, 14 (1976), 3110–3120.
[12] I. Dimitrović, P. Hasenfratz, J. Nager and F. Niedermayer, Finite-size effects, goldstone bosons and critical exponents in the $d = 3$ Heisenberg model, Nucl. Phys., B350 (1991), 893–950.

[13] J. Engels and T. Mendes, Goldstone-mode effects and scaling function for the three-dimensional $\mathcal{O}(4)$ model, Nucl. Phys., B572 (2000), 289–304.

[14] J. Engels, S. Holtman, T. Mendes and T. Schulze, Equation of state and goldstone-mode effects of the three-dimensional $\mathcal{O}(2)$ model, Phys. Lett. B, 492 (2000), 219–227.

[15] J. Engels and O. Vogt, Longitudinal and transverse spectral functions in the three-dimensional model, Nucl. Phys., B 832 (2010), 538–566.

[16] J. Kaupužs, R. V. N. Melnik and J. Rimšāns, Advanced Monte Carlo study of the Goldstone mode singularity in the 3D *XY* model, Commun. Comput. Phys., 4 (2008), 124–134.

[17] J. Kaupužs, R. V. N. Melnik and J. Rimšāns, Monte Carlo estimation of transverse and longitudinal correlation functions in the $\mathcal{O}(4)$ model, Phys. Lett. A, 374 (2010), 1943–1950.

[18] J. Kaupužs, Canadian J. Phys., 9 (2012), 373.

[19] J. Kaupužs, R. V. N. Melnik and J. Rimšāns, Goldstone mode singularities in $\mathcal{O}(n)$ models, Condensed Matter Phys., 15 (2012), 43005.

[20] J. Kaupužs, Longitudinal and transverse correlation functions in the φ^4 model below and near the critical point, Progress of Theoretical Phys., 124 (2010), 613–643.

[21] J. Kaupužs, Int. J. Mod. Phys., A27 (2012), 1250114.

[22] V. Dohm, Crossover from Goldstone to critical fluctuations: casimir forces in confined-symmetric systems, Rev. Lett., 110 (2013), 107207.

[23] P. Butera and M. Comi, Critical specific heats of the *N*-vector spin models on the simple cubic and bcc lattices, Phys. Rev. B, 60 (1999), 6749–6760.

[24] K. R. Ite and H. Tamura, Commun. Math. Phys., 202 (1999), 127.

[25] M. E. J. Newman and G. T. Barkema, Monte Carlo Methods in Statistical Physics, Clarendon Press, Oxford, 1999

[26] A. Erdélyi, Asymptotic representations of Fourier integrals and the method of stationary phase, J. Soc. Indust. Appl. Math., 3 (1955), 17–27.

[27] Fedoriuk, Asymptotics Integrals and Series, Nauka, Moscow, 1987.

[28] J. Kötzler, D. Görlitz, R. Dombrowski and M. Pieper, Z. Phys., B94 (1994), 9.